THE ASTROPHYSICAL JOURNAL, 385:501–511, 1992 February 1

AN IMPROVED METHOD TO DERIVE H I ABSORPTION SPECTRA THROUGH THE DISKS OF GALAXIES: APPLICATION TO THE SCULPTOR GROUP

JOHN M. DICKEY
University of Minnesota, 116 Church Street, S.E., Minneapolis, MN 55455
AND
ELIAS BRINKS AND DANIEL PUCHE
National Radio Astronomy Observatory, P.O. Box O, Socorro, NM 87801
Received 1991 April 15; accepted 1991 August 8

ABSTRACT

We study in detail the optimum technique for measuring λ21 cm absorption spectra with an aperture synthesis instrument. Using continuum sources behind galaxies in the Sculptor Group as examples, we derive formulae for the best estimate for the optical depth and the error on this estimate. In this case the dominant source of error is variation in the foreground H I emission of the disks of the galaxies, and we discuss how best to treat this problem. In addition to the absorption previously known toward the nucleus of NGC 253, new absorption is detected tentatively in one case in NGC 247. The H I gas in that case must be quite cool.

The absorption in the nucleus of NGC 253 is of particular interest. We estimate the spin temperature by interpolating the emission spectra over the area of the continuum emission. The atomic gas temperature is extremely cold, below 25 K at some velocities. The H I seen in absorption is probably in the molecular clouds in the nuclear region.

Subject headings: galaxies: individual (NGC 247, 253) — galaxies: ISM — radio continuum: galaxies — radio lines: atomic

1. INTRODUCTION

Absorption at λ21 cm by neutral hydrogen in the disk of a spiral galaxy provides a means of measuring the distribution of spin temperatures in the interstellar medium. Cool gas ($T \sim 100$ K) is seen in absorption and emission in this line, whereas warmer gas (typically at 6000 to 10,000 K) shows only emission. Comparing emission and absorption spectra from the same vicinity thus provides a measure of the amount of gas in the cool and warm phases of the neutral atomic component of the ISM. Many studies have been performed in our galaxy showing that in the solar neighborhood typically 50% to 75% of the atomic hydrogen is warm (reviewed by Dickey & Lockman 1990).

In other galaxies 21 cm absorption has been studied most often toward the continuum emission from active nuclei (e.g., van Gorkom et al. 1989; Dickey 1986, and references therein). This preferentially selects gas in the nuclear regions of Seyfert and starburst galaxies, which may not be typical of the normal interstellar media of quiescent spirals. In order to address questions of how the distribution of interstellar gas temperature varies with galactic radius, morphological type, or overall star-formation rate, for example, we must find a way to sample random directions through the disks of nearby spirals.

There are several background radio continuum sources behind any nearby galaxy disk, but they are typically faint (a few mJy), so that very sensitive measurements are required to detect even the deepest absorption lines. A more important limitation on sensitivity of H I absorption spectra is not ordinary noise but the fluctuations of the 21 cm emission in front of the background source. How severely the emission pollutes an absorption spectrum depends on the flux and angular size of the background source, and the beam size of the telescope. Only the VLA[1] has a sufficiently small beam to be able to measure absorption toward the typical extragalactic background source found behind even the largest, most nearby spiral disks. A small beam is doubly an advantage. First, it allows measurement of the emission much closer to the background source, so that the interpolation to find an "expected emission" profile is more precise. Second, because the VLA is an interferometer it acts as a spatial filter, reducing and often eliminating the contribution of H I seen in emission in front of the source. The strength of the emission which mixes with the spectrum of the continuum is proportional to the emission brightness times the beam solid angle. Typically the emission brightness temperature is lower than 125 K in the Milky Way (175 K in M31, Braun & Walterbos 1991). With a 15″ beam (Gaussian FWHM), emission with a brightness temperature of 50 K contributes 19 mJy beam^{-1}, typical for the maximum seen by an 8 km s^{-1} channel. In contrast a 3″ beam observing the same emission would only see 0.7 mJy beam^{-1}. Some of this can be estimated by interpolation and subtracted; this works very effectively for the Milky Way gas, which is smoothly spread over angles smaller than a few arcmin. Other galaxies have stronger emission fluctuations on smaller angular scales than the foreground Milky Way gas since they are so much more distant; typically spatial variations cause such interpolation to be uncertain by 10% or more of the total.

To date, the only galaxy for which many lines of sight have been studied in absorption with the VLA is M31 (Dickey & Brinks 1988; Braun & Walterbos 1991). In the project reported

[1] The VLA is part of the National Radio Astronomy Observatory, which is operated by Associated Universities, Inc., under coperative agreement with the National Science Foundation.

here we search for absorption toward continuum sources behind five spiral galaxies in the Sculptor group, NGC 55, NGC 247, NGC 253, NGC 300, and NGC 7793, by reanalyzing the data taken in the emission surveys of Puche (1990). These data were taken with the VLA C and D arrays, giving typical beam sizes of 25″. They have thus provided excellent maps of the 21 cm emission. However, this resolution is marginal for removing the emission fluctuations to allow sensitive absorption spectra to be measured toward continuum sources of 5 to 10 mJy. In § 2 (Analysis) we discuss the analysis method with emphasis on the estimation of errors in the derived optical depth, τ. We present there the best candidates for detection of absorption, and the upper limits on τ for the other lines of sight sampled. In § 3 we discuss the astrophysical conclusions that can be drawn from the results here, and the best observational strategies to obtain better measurements of the temperatures in the disks of nearby spirals. The case of the nuclear source in NGC 253 is special, and we discuss that in detail in § 5.

2. ANALYSIS

The observations and data reduction are described in a series of papers on the individual galaxies (Carignan & Puche 1990a, b; Puche, Carignan, & Wainscoat 1991; Puche, Carignan, & van Gorkom 1991; and Puche Carignan, & Bosma 1990). The velocity resolutions and ranges covered by the cubes are listed on Table 1. The field center positions are also given on Table 1.

Absorption studies begin with the selection of suitable continuum sources. Since these galaxies are at high galactic latitudes, we are quite confident that all the continuum sources are extragalactic, and so must be either intrinsic to the galaxies of interest, or more likely far behind them. We have fitted the peaks of the compact continuum sources with paraboloid or Gaussian models to determine the center positions and peak fluxes. These are listed on Table 2. In many cases the continuum sources are well outside the H I emission. It is interesting to search these lines of sight for absorption just in case there are small, cold clumps of gas far outside the main H I disks. On Table 2 the sources without entries in the sixth column (S_{em}) are the ones outside the H I disks; there are 18 of these, of which seven have rms noise in optical depth of 0.07 or less, giving upper limits to the optical depth of 0.25 or less. We detected no absorption along any line of sight outside the area of H I emission from the galaxies. Although the flux of some sources seemed to decrease over some range in velocity, careful inspection showed that this was due to imperfections in the cleaning of the very extended emission which left a "bowl" around the emission, mimicking the effects of absorption. These can be distinguished from real absorption because they typically extend beyond the continuum source.

For background sources behind the H I disks the determination of the optical depth spectrum is much more complicated. There are two issues: how to combine the spectra toward the several pixels in which the continuum is strong to get the best estimate of the "on-source" spectrum and how to use the emission spectra toward the nearby pixels where the continuum is weak to get the best estimate of the "expected emission" spectrum toward the source. If the continuum were strong and very compact, and the emission were smoothly distributed over several beam areas, then many different methods would give the same result (e.g., Gaussian fitting of the source in each channel or summing pixels in an area surrounding the peak of the source in each channel). Unfortunately the continuum is often very faint and the H I emission varies considerably across the beam, so that different techniques can give discrepant results. For the maps in our study the beam is fairly large. In order to make a meaningful analysis we have developed an improved method to remove the emission and to derive the absorption spectrum. These improvements include a scheme to do a weighted average over the continuum source and an accurate determination of the uncertainties in the final absorption profile, combining the effects of thermal noise with the uncertainty arising from the way the expected emission was determined. For the latter issue we present two alternative interpolation methods.

Figure 1 illustrates the problem. The contours show the continuum as measured by the VLA beam. Superposed on the contours are spectra for each pixel. Pixels with a continuum level above 50% of the continuum peak (obtained from paraboloid fitting) have spectra with short vertical bars on either side with height 50 mJy. Pixels with continuum level lower than 10% of the continuum peak have spectra without end bars. Pixels with a continuum between 10% and 50%, and pixels further than 65″ from the continuum peak have no spectra drawn, nor are they used in the analysis. The objective is to combine these two groups of pixels in such a way as to get the best possible estimate of the optical depth and an assessment of the uncertainty in the optical depth at each velocity.

In the simplest case of perfectly smooth line emission, so that the line emission toward the continuum can be estimated exactly, the absorption would be given by

$$e^{-\tau} = \frac{T_{\rm cont} + (T_{\rm on} - T_{\rm off})}{T_{\rm cont}}, \quad (1)$$

where $T_{\rm off}$ is the estimate for the on-source emission from interpolation of the off-source line emission and $T_{\rm on}$ is the measured spectrum in the direction of the source. Aperture synthesis instruments are generally calibrated by reference to unresolved point sources, so instead of dealing with brightness temperature in Kelvins, their maps are expressed in units of Jy per beam area for each pixel. Pixels containing continuum emission from the background source but no line emission or

TABLE 1

OBSERVATIONS OF SCULPTOR GROUP GALAXIES

Name	(1950) α	(1950) δ	v(center) (km s^{-1})	v(width) (km s^{-1})	Δv(channel) (km s^{-1})	Clean Beam	Gain (K mJy^{-1})
NGC 55	00^{h}12^{m}24^s.0	−39°28′00″	125	320	10.3	45″ × 45″	0.30
NGC 247	00 44 40.0	−21 02 12	165	320	10.3	33 × 21	0.87
NGC 253	00 45 07.0	−25 33 42	245	640	20.6	68 × 32	0.28
NGC 300	00 52 31.0	−37 57 24	145	320	10.3	17 × 12	2.97
NGC 7793	23 55 15.2	−32 52 10	230	320	10.3	44 × 33	0.42

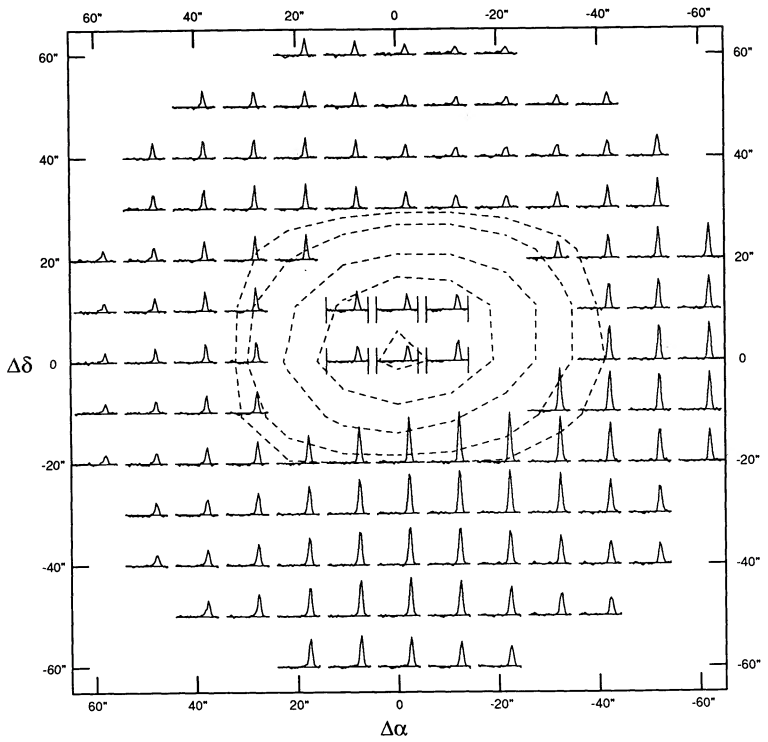

FIG. 1.—Spectra of the λ21 cm line from NGC 247, in the vicinity of background source 2 (Table 2). The contours show the intensity of the continuum emission with contour levels 5%, 10%, 25%, 50%, and 90% of the peak flux (41.5 mJy). Superposed on the continuum map are the spectra from each pixel of the spectral line cube, spaced in a 10″ × 10″ grid. Only spectra which contribute either to the aggregate absorption or emission are shown; pixels outside the radial distance cutoff (here 6.5 pixels, or 65″) are excluded, as are pixels where the continuum is between 10% and 50% of the peak. Spectra toward pixels with continuum above 50% of the peak are averaged, weighting by the continuum squared (s_i in eq. [2]). These are distinguished by short end bars, of height ±50 mJy per beam. Spectra toward pixels with continuum below 10% of the peak are used for the interpolation of the line emission over the area of the continuum. There is clear variation of the strength and center frequency of the emission over this area, so the method of interpolation used is crucial to determining the emission contribution to the on-source spectra. The clean beam size is slightly smaller than the extent of the source shown here (33″ × 21″).

absorption (at frequencies away from the H I line) then have brightness c_i instead of $T_{\rm cont}$, and pixels with line emission have brightness spectra which we will express as s_i. Toward the continuum source s_i includes emission and absorption, but the continuum level c_i has been subtracted.

The spectra toward the background source are averaged, weighting by the square of the continuum strength. Note that even an unresolved source will present several pixels above the 50% threshold, since the clean beam has typically 2.5 to 3 pixels full width at half maximum. These several pixels will not have identical spectra, since the emission nearby to the background source will blend differently with the continuum in each, even if the continuum is itself unresolved. The spectrum toward each pixel with continuum constitutes an estimate of the optical depth on-source; to obtain the best estimate of the optical depth spectrum we divide each by the continuum in that pixel before averaging. So the final optical depth spectrum is

$$\langle e^{-\tau}\rangle = \sum_i \left[\left(\frac{c_i^2}{\sum_j c_j^2}\right) \times \left(1 + \frac{s_i - s_{{\rm off};i}}{c_i}\right)\right], \qquad (2)$$

where s_i is the spectrum toward the ith on-source pixel with continuum subtracted, c_i is the continuum flux of this pixel, and $s_{{\rm off};i}$ is the interpolation of the off-source spectra giving the estimated emission in the direction of the ith on-source pixel. The summations run over all on-source pixels, i.e., those with c_i greater than 50% of the maximum c_i. Note that τ, s_i, and $s_{\rm off}$ are functions of velocity while c is just a number for each pixel.

The first term inside the summation in equation (2) is a weighting factor, which is chosen to minimize the noise in the resulting average spectrum. This error in $e^{-\tau}$ has two components: the radiometer noise and the noise due to emission fluctuations. Each of these contributes to the optical depth noise in each single pixel spectrum in proportion to c_i^{-1}. The optimum weighting is thus c_i^2, which is proportional to the inverse of the variance (σ_i^2) of each spectrum.

Before we can compute τ we must analyze the distribution of the emission spectra to obtain an interpolated estimate for the emission in each on-source pixel, $s_{{\rm off};i}$ above. This is the heart of the problem. As can be seen in Figure 1, the emission varies over the field, so the choice of mathematical technique used for the interpolation may influence the resulting optical depth spectrum. In fact, it influences it severely. This can be seen in Figures 2–5, which show the same field after subtracting four different models for the emission. Figures 2 and 3 were made by fitting a bilinear function to each spectral channel, i.e.,

$$s_{\rm off}(x, y; v) = [a(v) \times x] + [b(v) \times y] + c(v)\,,$$

where x and y are coordinates on the plane of the sky. The only difference between Figures 2 and 3 is the range of off-source pixels contributing to the least-squares fit for a, b, and c; for Figure 2 pixels are accepted out to a radius of 6.5 pixels from the continuum peak (as long as they have continuum flux less than 10% of the peak) and for Figure 3 the radius is 4.5 pixels (10″ per pixel). Since it is the residual around the fit which is plotted, the mean over all off-source pixels must be zero, which

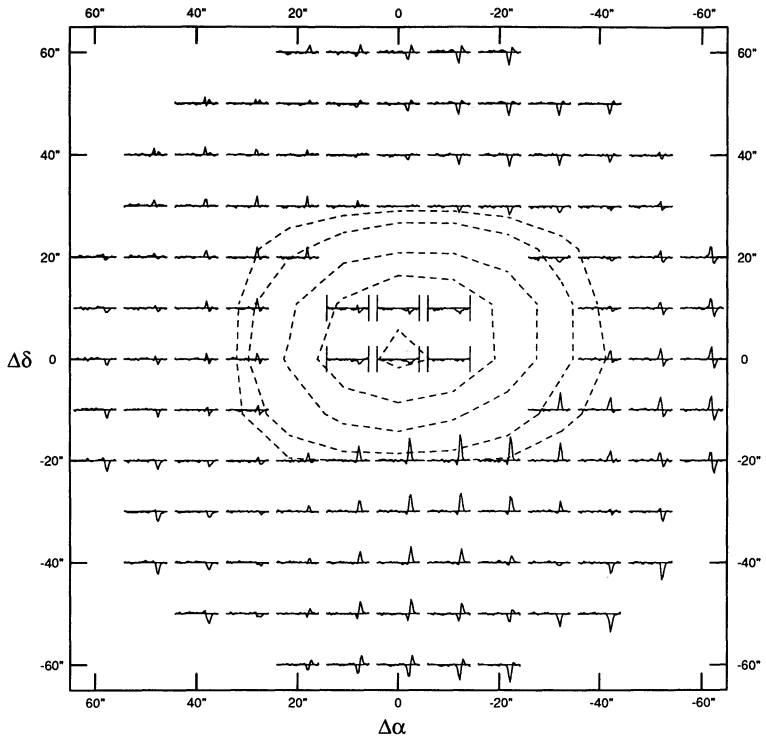

FIG. 2.—Residuals after fitting the emission spectra of Fig. 1. Here a bilinear fit has been subtracted from all spectra. For each velocity channel of the spectrum, a linear function of $\Delta\alpha$ and $\Delta\delta$ (x and y in the text) has been least-squares fitted using only the spectra without end bars on Fig. 1, i.e., those where the continuum is below 10% of the peak. These fits are done independently for each channel, and subtracted from the data to leave the residuals shown here. The bilinear function value for positions in front of the continuum is subtracted from those spectra as well. If the interpolation were perfect this would remove all the emission from the on-source spectra, leaving only the absorption. The fact that there are significant residuals in the off-source spectra shows that the fit is not perfect, because the variation of the emission is more complex than a simple bilinear function. The magnitude of these residuals off-source provides an estimate of the error in the interpolated spectra, and hence the error in the resulting optical depth spectra.

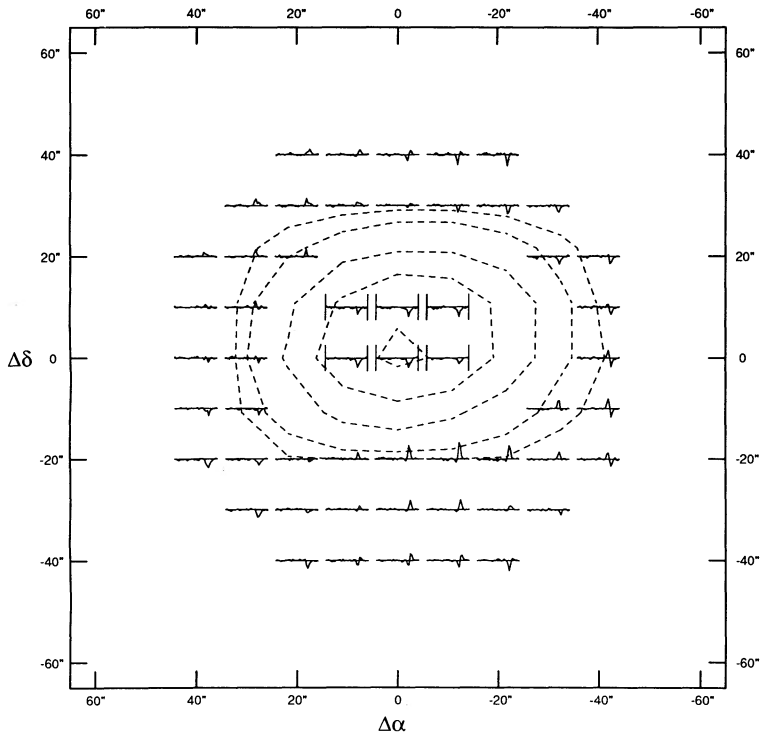

FIG. 3.—Residuals from a bilinear fit with maximum radius 45″. This is similar to Fig. 2, except here the least squares fit is made only to spectra toward pixels within 45″ of the peak of the continuum. The residuals after subtracting this fit are shown. Restricting the area over which the least squares fit is done reduces the residuals because a bilinear function is a better model of the emission variation on a smaller scale.

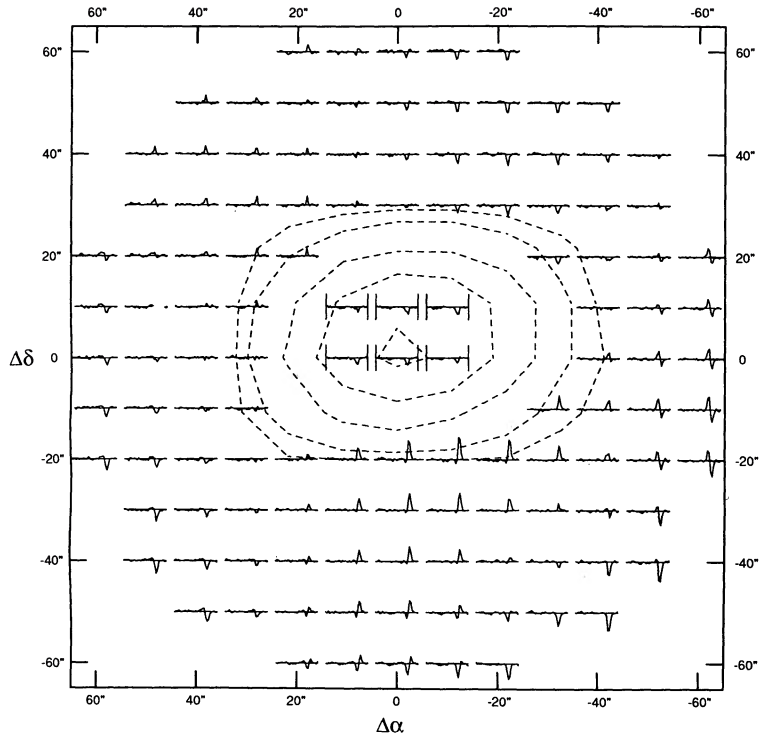

FIG. 4.—Residuals after interpolation of Gaussian fit parameters. In this case the interpolation is done not by fitting each spectral channel with a bilinear function, but by first fitting each emission spectrum with a Gaussian line profile. The three parameters of these fits (amplitude, center velocity, and velocity width of the emission toward each pixel) are then fitted spatially with bilinear functions. As in Fig. 2, the radial range contributing to the fit is 65″ around the continuum peak. The residuals here are surprisingly similar to those shown on Fig. 2.

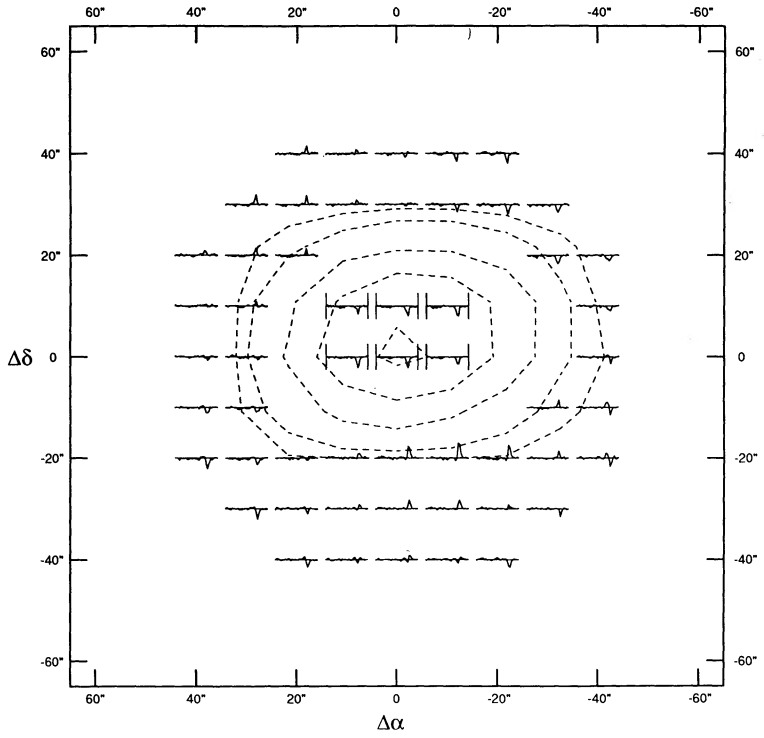

FIG. 5.—Residuals of Gaussian interpolation over a 45″ range. The method used here is the same as in Fig. 4, but the range over which the fit is taken is only 45″, as for Fig. 3. Again, the residuals here are surprisingly similar to those on Fig. 3.

explains the roughly equal number of positive and negative "lines" coming from variations in the peak of the emission; the "S" shaped profiles result from a shift in the center velocity of the emission line. Although this pattern is similar in the two figures, the on-source spectra are noticeably different, as they are now the difference between the observed spectrum and the interpolation, i.e., $s_i - s_{\mathrm{off};i}$.

Physically the variations in emission are better understood in terms of variations in the height, center velocity, and width of the emission line, rather than many independently varying channels. This suggests that a better approach to the interpolation is to fit all the off-source spectra with Gaussians, and then interpolate the Gaussian parameters with bilinear fits. That is what is done in Figures 4 and 5, again with the two different cutoffs in separation from the source. The results are somewhat more stable than the channel by channel interpolation, in that the on-source spectra now vary less with the cutoff distance. This method is also to be preferred because there are many fewer fitted parameters, nine rather than 93. But it is disturbing that the result is so sensitive to the method of fitting, obviously we need to determine a confidence envelope around the optical depth spectrum which takes account of the variation of the emission.

Figure 6 shows the emission and absorption spectra resulting from the four interpolation methods shown on Figures 2–5. Each panel of Figure 6 shows an emission spectrum and an absorption spectrum ($e^{-\tau}$) with error envelopes which reflect the spatial fluctuations of the emission more than anything else. The emission spectrum is the expected emission at the position of the continuum source based on the particular interpolation method used and calculated using the same weighting area and weights as used for calculating the absorption spectrum, i.e.,

$$s_{\mathrm{em}} = \frac{\sum s_{\mathrm{off};i} \times c_i^2}{\sum c_i^2}, \tag{3}$$

where the summation is taken over the pixels with c_i greater than 50% of the peak, as for the absorption. The error envelope on the emission spectrum is plus and minus the rms in each channel of the residual emission computed using all off-source pixels which are used for the interpolation, i.e.,

$$S_{\mathrm{rms}}(v) = \sqrt{\frac{1}{n} \sum [S_i(v) - S_{\mathrm{off};i}(v)]^2}, \tag{4}$$

where the sum is taken over the n off-source pixels. This is a conservative estimate of the error in the interpolated emission; one might well argue that a better, albeit more optimistic, estimate of the true error would be S_{rms} divided by the square root of the number of independent measurements contributing to the n off-source pixels, which is about $n/6$, as it would be if we simply wanted to estimate the mean emission.

The error bars on the absorption spectrum vary with velocity to reflect the shape of S_{rms}. This envelope is given by one plus and minus τ_{rms}:

$$\tau_{\mathrm{rms}}(v) = \frac{S_{\mathrm{rms}}(v)}{c_{\max}} \tag{5}$$

where $c_{\max}$ is the value of the continuum in the highest pixel. This is a conservative estimate of the error in $e^{-\tau}$, since for a resolved source we have a better estimate of the absorption than just represented by the peak pixel spectrum. A more

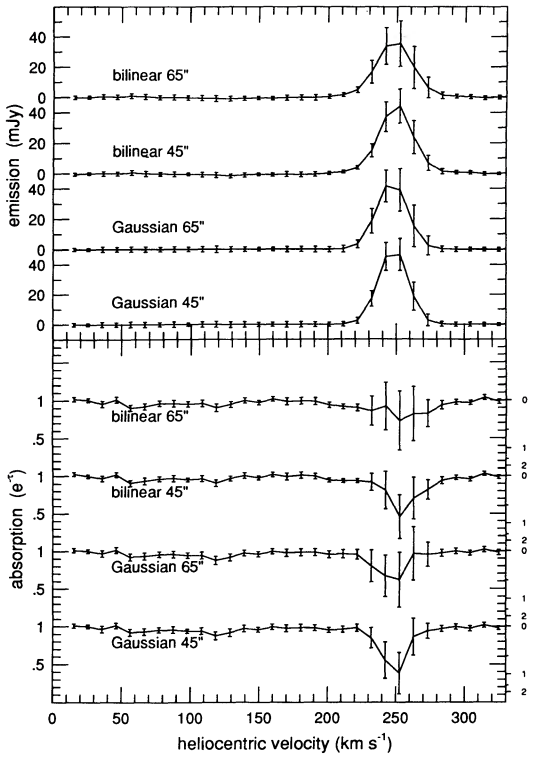

FIG. 6.—Spectra toward the second continuum source in NGC 247 resulting from the interpolations illustrated on Figs. 2–5. Above are four estimates for the emission (scaled in mJy beam^{-1}) averaged over the area of the continuum source, weighting by continuum squared, for the six "on-source" pixels where the continuum is above 50% of the peak. The error bars on these are plus and minus 1 σ predicted on the basis of the residuals of the emission fit to the off-source pixels (eq. [4]). Below are shown the corresponding optical depth spectra, derived by subtracting the interpolated emission from each on-source pixel, dividing by the corresponding continuum, and averaging the result with appropriate weights (eq. [2]). Fractional absorption is scaled on the left, optical depth is scaled on the right. The errors in optical depth resulting from errors in emission interpolation (eq. [5]) are shown as plus and minus 1 σ error bars on each point. Even though the emission seems to be reasonably well determined in the spectra above, the errors in the fit have a tremendous effect on the absorption spectra. Only in the 45″ cases could a detection be claimed at all, and clearly parameters of the absorption line are very poorly determined.

liberal determination of the optical depth noise resulting from S_{rms} would be to divide by $\sum c_i$ and simultaneously multiply by the number of pixels per beam area, since the total continuum flux density is usually better estimated by this ratio than by the peak alone. Note that for small optical depth $\tau \simeq 1 - e^{-\tau}$, so τ_{rms} is an estimate of the noise in either τ or $e^{-\tau}$, although for deep absorption lines the error in τ is actually $\tau_{\mathrm{rms}} \times e^{+\tau}$.

In the case of the continuum source analyzed in Figures 1–6 we can claim at least a tentative detection of absorption as for both the channel to channel and the Gaussian interpolations with 4.5 pixel cutoffs the absorption is deeper than 2 τ_{rms}; on Figure 5 we find $e^{-\tau} = 0.38 \pm 0.27$, corresponding to $\tau = 1.0 \pm 0.7$. In the absence of emission fluctuations this error would be much smaller. The value of S_{rms} measured over several off-line channels is only 2.0 mJy, which gives the radiometer noise level. That would give only 0.04 for τ_{rms} since for this source $c_{\max}$ is 41.5 mJy.

The point of this analysis is to underline the uncertainties in absorption spectra measured with resolutions of 20″ or larger (VLA C and D arrays). The errors introduced by emission variations are similar to the "pseudo-absorption" which

limited galactic absorption studies with resolutions of 10′ or more (Radhakrishnan et al. 1972). Such problems persist for single dish studies of galactic absorption at low latitudes. However, although individual spin temperatures may be poorly determined it is still possible to learn much about the thermodynamic state of the gas in spite of emission fluctuations (e.g., Colgan, Salpeter, & Terzian 1988; Kuchar & Bania 1990). For studies of absorption in nearby galaxies such as these, higher resolution observations such as that of the VLA in A array can largely eliminate the emission, so absorption spectra measured in that way could be much more accurate than those obtained here.

3. RESULTS

Having explored the possibilities for interpolating the emission spectra to get an optimum estimate of absorption we apply these techniques to the continuum sources behind the Sculptor group. In most cases we use the simple bilinear fit to each channel, but in cases where there are suggestions of absorption we use both methods, with several cutoff radii. The continuum sources toward which we have searched for absorption are listed on Table 2. Many of these are outside the detected H I emission from the galaxies, but they are of interest to search for small clouds of cold, atomic gas in either very extended disks or halos of the galaxies such as those responsible for some Na and Ca absorption lines toward quasars (see Corbelli & Schneider 1990). No absorption has been detected toward continuum sources outside the H I emission. Column (4) of Table 2 lists the background source peak flux density and column (6) gives the peak emission. Column (5) gives the maximum rms optical depth ($e^{-\tau} \sim \tau$) at the velocity of the most extreme fluctuations of the emission. Column (7) gives the rms fluctuations of the emission over the field (within a radius of 6.5 pixels of the continuum source), or the rms noise in cases where no emission is detected.

Most of the continuum sources behind emission show no absorption. Unfortunately, most of these do not set very significant limits on the spin temperature, since the emission fluctuations cause the noise in the optical depth to be large. The minimum values of the spin temperature implied in each case where emission is detected are given in the last column of Table 2. These are derived by converting the emission brightness to a brightness temperature and dividing that by twice the noise level in the optical depth spectrum. The spectra toward the 27 mJy source behind NGC 55 (the sixth entry on Table 2 for NGC 55) are shown in Figure 7. Here the errors in absorption are quite large. There may be an absorption line on the high velocity side of the emission (150–165 km s^{-1}), but the emission fluctuations are so great here that the line is not reliable. At lower velocities where the emission is stronger (130 km s^{-1}) the nominal value for the spin temperature is 180 K, but taking a reasonable upper limit for τ gives only 60 K. Similar values come from the 41.5 mJy source behind NGC 247 shown on Figure 6 at the peak of the emission. If the absorption in that case is real it suggests quite cold temperatures, $T_{\rm spin} = 25$ K, although the error bars are so large that the 1 σ range of spin temperatures is 16 to 50 K.

The conclusions from this study are that there are few lines of sight through these galaxies with very cold gas ($T_{\rm spin} < 25$ K, say), but we do not learn how much H I is in the cool phase (50 to 100 K) versus how much is in the warm phase (6000 to 10,000 K), which is the important issue for interstellar thermodynamics. It is not surprising that we detect so little deep absorption in light of what is known about the phase balance

TABLE 2

CONTINUUM SOURCES SEARCHED FOR ABSORPTION

Galaxy (1)	(1950) α (2)	(1950) δ (3)	S_c (mJy beam^{-1}) (4)	$\tau_{\rm rms}$ (5)	$S_{\rm em}$ (mJy beam^{-1}) (6)	$S_{\rm rms}$ (mJy beam^{-1}) (7)	$T_{\rm min}$ (K) (8)
NGC 247	00^{h}45^{m}24^s.3	−20°54′14″	134.1	0.02	...	2.4	
	00 44 44.9	−21 07 37	41.5	0.29	47	2.0	70
	00 44 53.8	−21 17 45	62.8	0.07	...	3.1	
	00 43 59.2	−21 03 58	18.8	0.13	...	2.4	
	00 43 22.5	−20 57 30	17.6	0.29	...	3.5	
	00 44 20.9	−20 58 54	5.8	0.38	35	1.6	40
	00 44 41.5	−20 55 05	5.6	2.30	48	1.6	...
NGC 253	00 45 05.7	−25 33 39	1535	0.02	32	4.9	224
	00 45 31.5	−25 34 48	46.8	0.13	...	4.8	
	00 43 55.0	−25 35 56	53.0	0.16	...	8.0	
	00 43 40.0	−25 28 21	51.8	0.23	...	8.6	
NGC 300	00 51 41.6	−38 02 50	315.0	0.03	...	6.3	
	00 51 31.0	−37 56 32	268.0	0.05	...	9.4	
	00 52 32.6	−37 52 12	10.7	0.22	18	1.2	121
NGC 55	00 10 29.1	−39 38 34	113	0.07	...	5.5	
	00 09 30.7	−39 16 00	49.5	0.30	...	8.7	
	00 12 28.5	−39 29 11	38.2	0.84	220	3.8	...
	00 09 45.2	−39 20 46	35.6	0.25	...	4.7	
	00 13 37.8	−39 33 18	33.9	1.77	238	17.3	...
	00 12 44.0	−39 27 28	27.4	0.30	61	3.0	30
	00 09 56.6	−39 29 06	29.5	0.20	...	4.4	
NGC 7793	23 55 56.9	−32 55 01	83.5	0.03	...	2.5	
	23 53 55.6	−32 38 59	220.5	0.04	...	5.9	
	23 53 51.5	−33 06 56	146.2	0.07	...	6.6	
	23 55 03.6	−33 08 56	18.7	0.25	...	3.3	
	23 54 41.2	−32 40 48	13.2	0.28	...	2.1	
	23 54 56.1	−32 54 11	6.0	1.50	24	2.4	...
	23 55 25.5	−32 50 00	5.9	1.70	41	1.3	...

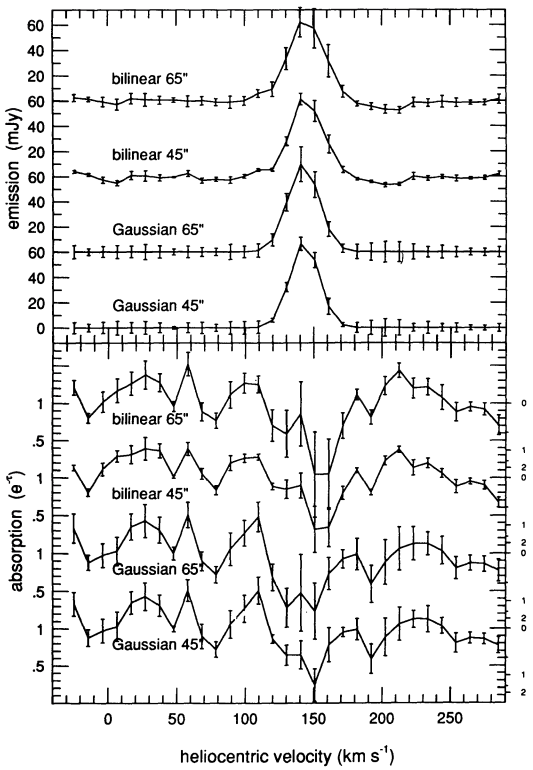

FIG. 7.—Spectra toward the sixth continuum source in NGC 55, in the same format as on Fig. 6. The noise level is higher here, and the continuum is weaker, so the data are insufficient to determine whether there is absorption or not, even though the emission is smoothly distributed. Note that the interpolation is fairly accurate, at least in the 45″ cases, as seen in the small error bars on the emission spectra.

in the Milky Way. The solar neighborhood has roughly 30% to 35% cool H I, and the rest warm, assuming an excitation temperature of 75 K for the cool gas. The minimum spin temperatures on Table 2 are typically less than 75 K, so in fact there would have to be very cold H I on these lines of sight in these galaxies to be detectable in absorption. It is of interest to learn that the covering factor of very cool gas in the Sculptor galaxies is *not* high (as may be the case in some spirals as suggested by Shaya & Federman 1987); but there is no evidence from our results that these galaxies differ from the Milky Way. A striking exception is the nucleus of NGC 253, as discussed in the next section.

4. THE NUCLEUS OF NGC 253

The emission and absorption toward the nuclear source in NGC 253 is shown in Figure 8. The 21 cm absorption in this case has been known since Gardner & Whiteoak (1974), with a previous interferometer study made by Gottesman et al. (1976) and Combes et al. (1977). Spectra of many molecular and atomic species are available as well (Turner 1985; Canzian, Mundy, & Scoville 1988; Baan et al. 1990; Sage, Shore, & Solomon 1990, and references therein). We shall consider here the cold atomic gas in and in front of the nucleus, using our emission and absorption data to derive the spin temperature of the gas. This is difficult because it requires both good sensitivity in emission and high dynamic range and moderately high resolution to separate the emission from the absorption around the continuum. In addition, the large angular extent of the continuum (2′ × 7′ at a level of 10 K surface brightness, Turner 1985) makes interpolation of the emission across the face of the absorption very uncertain. This interpolation is required to derive the spin temperature, since this calculation assumes that the emission and absorption correspond to the same gas. Equipped with the several interpolation techniques described above we shall attempt this calculation, paying particular attention to the scale of errors expected due to inaccuracy of the interpolated emission spectrum.

There is no problem in determining the absorption quite accurately in spite of inaccuracies in the interpolation of the emission, since the continuum is so strong that the error due to the emission fluctuations makes only a slight difference in the optical depth. The four different methods of interpolating the emission over the continuum source are presented on Figure 8 in the same way as on Figure 6. The bilinear and Gaussian fits give almost identical results for $e^{-\tau}$. In Figure 8 we have subtracted the interpolated emission from the spectrum on-source before dividing by the continuum, as prescribed in equation 2; but, as the error bars suggest, this subtraction makes little difference since the continuum is so strong.

The estimates for the emission averaged over the area of the source coming from the various interpolation methods differ substantially. The Gaussian fits give a poor representation of the line profile in this case since there are broad, roughly exponential wings on the emission. The bilinear fits give better estimates of the line shape, but more error in the interpolation because the spatial variation is difficult to model with a linear function in each channel. The spatial structure is better modeled with smooth functions for the line center, width and

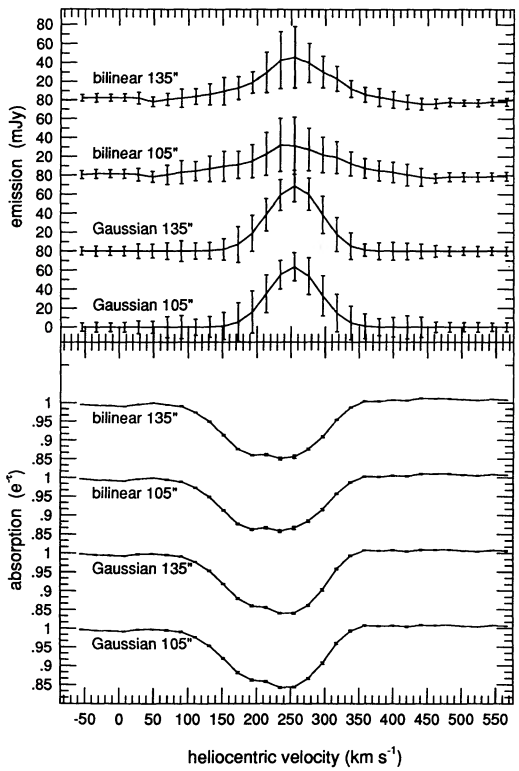

FIG. 8.—Spectra toward the nucleus of NGC 253 (the first continuum source on Table 2). In this case the continuum is strong, so the optical depth is very well determined, in spite of uncertainties in the interpolation of the emission over the large area of the continuum. Note that the radial ranges of the fitting regions have been increased to 135″ and 105″ from the continuum peak.

height, but there is clearly more structure on small scales than can be fitted by linear interpolation over the entire area of the continuum source. The continuum is so extended that we take larger areas for the interpolation (105″ and 135″, beyond even the 5% level, since the peak flux is so high). The direction of the effect is that the smaller the area used, the higher the peak of the emission, which indicates that there is a concentration of gas in front of the nucleus which does not fully extend to the area around the continuum.

In Figure 9 we show again the results of the two bilinear fits to the emission distribution, with the corresponding estimates for the absorption, and the derived spin temperature below. Here the emission is converted to units of brightness temperature, and the absorption is plotted upside down ($1 - e^{-\tau}$). The absorption spans almost the entire velocity range covered by emission, about 75 to 330 km s^{-1} in absorption versus 75 to 400 km s^{-1} in emission. This is broader than the emission or absorption seen in most molecular species, but not as broad as the λ18 cm OH, which extends from 60 to 550 km s^{-1} in absorption (Turner 1985).

The center of the absorption line is at about 212 ± 5 km s^{-1} whereas the emission is centered at about 240 ± 5 km s^{-1}, which is similar to what is seen in molecular emission; the emission from CS and CO peak above 250 km s^{-1}. A simple interpretation of this velocity offset is that there is a velocity difference between the near side of the nucleus and the far side.

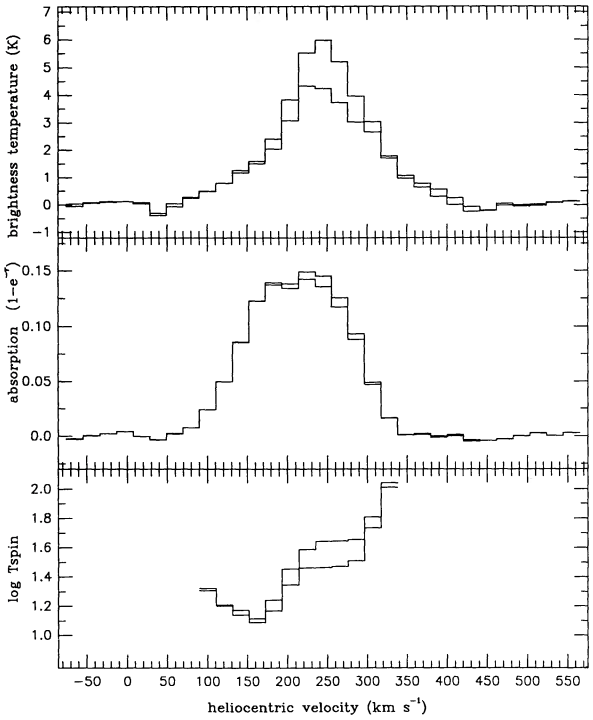

FIG. 9.—Derivation of the spin temperature in the nucleus of NGC 253. In this case the two bilinear fits to the emission are plotted together on the upper spectrum. They show more variation than the Gaussian fits, so their difference is a pessimistic estimate for the error in the emission estimate. The two corresponding absorption spectra ($1 - e^{-\tau}$, with absorption going up) are plotted in the middle. From these the spin temperature in each channel is derived, as shown in the lower spectrum. Errors in the upper spectra propagate to the errors shown by the two values shown for each channel. The resulting temperatures are extremely cold for atomic hydrogen, at least by galactic standards, particularly at the lower velocities.

Only the near side contributes to the atomic and molecular absorption, of course, while both sides contribute to the emission. The offset of the H I lines suggests outflow at about 15 km s^{-1}. This interpretation was suggested qualitatively by Gottesman et al. (1976). The molecular absorption lines seen in OH and H_2CO (14.5 GHz, Baan et al. 1990) complicate this interpretation. The OH in particular shows kinematic structure different from that of the H I in the inner 10″ to 15″, so comparison between the species is complicated.

The spin temperature, i.e., the ratio of the first two spectra, is plotted on the lower panel of Figure 9. This is the excitation temperature of the H I line, a good measure of the kinetic temperature of the gas. It varies from about 105 K (103 and 110 in the two interpolations) down to about 12.8 K (12.3 to 13.0). The coldest gas is at about 165 km s^{-1}. The gas at velocities above 350 km s^{-1} must be warmer than about 125 K, since the rms in the absorption spectrum σ_τ is 2×10^{-3}, and the absorption is well below two sigma, while the emission is about 0.5 K.

The variation of spin temperature with velocity may be real, or it may be an observational result of mixing two or more components of gas with very different temperatures. Warm gas ($T \gg 150$ K) would not contribute to the absorption spectrum. If there were a mixture of warm and cool gas which changes with velocity (cool gas predominating at lower velocities, warm at higher velocities) this would explain the spin temperature profile. However the spin temperature is already so low at 165 km s^{-1} that there cannot be much warm gas blended with the cold gas at this velocity, since that would require that the kinetic temperature of the cold H I be even lower than what we measure. At 13 K this gas is dramatically colder than any spin temperature measured anywhere in the Milky Way; it is hard to imagine that this number comes from a blend of even colder gas with warm gas. The coldest measured Milky Way spin temperatures are roughly 25 K, e.g., in the direction of 3C 225 (Knapp & Verschuur 1972).

These extremely low spin temperatures can be put off if we invoke drastic emission variations in front of the nucleus. As suggested above, there may be considerably more H I in front of the continuum than there is around it, so that the actual on-source emission spectrum would be higher than the interpolated estimate. Even imagining that it is twice as strong as estimated ($T_B = 3$ K, rather than 1.5 K at $v = 165$ km s^{-1}, for example) this would raise the spin temperature by only a factor of two (from $T_{sp} = 12.5$ K to about 25 K). This is close to the kinetic temperature used to model the molecular emission and absorption. The OH maser requires infrared pumping (Turner 1985) which probably comes from a warm dust population heated by the active nucleus (see Puxley, Hawarden, & Mountain 1990 for a recent discussion of models). In this environment, 25 K seems like a minimum reasonable value for the H I spin temperture, we cannot rule out the possibility that T_{sp} is that high with the present data. On the other hand, if the column density of gas varies by a factor of 2 or more over the continuum source we should see variations of the absorption between the nucleus itself, which has a compact continuum source of very high brightness, and the more extended continuum associated with the active star-formation region (see Turner & Ho 1983, for spectral index mapping). Observations with higher resolution might help to clarify the small scale structure of the column density and spin temperature in front of the continuum, and so more precisely constrain the spin temperature.

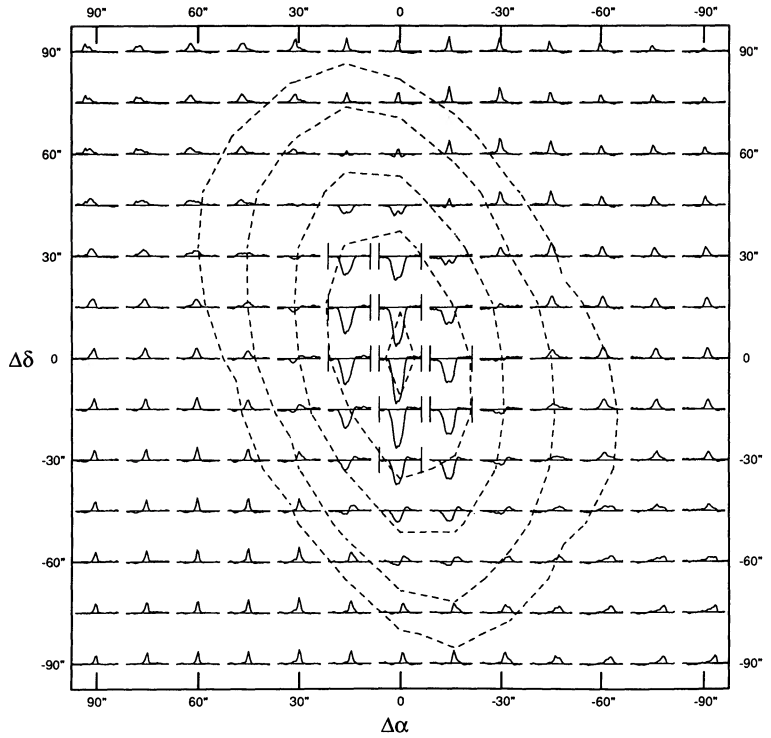

FIG. 10.—All spectra toward the nucleus of NGC 253. In this case all spectra are shown, not just those contributing to the emission and absorption estimates. The pixel size here is 20″. Spectra toward pixels with continuum above 50% of the peak have end bars of height 200 mJy beam^{-1}. No subtraction of emission has been made here. The division of the absorption profile into two separate velocity components, corresponding to the two spin temperatures on Fig. 9, is evident, particularly on the northern side of the continuum.

The resolution obtained here is not fine enough to make a detailed map of the absorption structure, but we do have several resolution elements across the continuum. Figure 10 shows the variation of absorption and emission over this area. The variation most apparent is not a concentration of gas toward the center, but rather a shift in the importance of two separate components of the absorption line. One centered at about 165 km s^{-1} varies more rapidly than the other, centered at about 225 to 235 km s^{-1}, which is fairly constant over the source. The lower velocity line apparently corresponds to the very cold gas; it is deeper on the east side of the continuum than on the west. The higher velocity line has spin temperature about 45 K. Only this higher velocity gas shows H_2CO absorption (Baan et al. 1990).

This kinematic structure in the H I is different from what is seen in OH and in the optical, explained by Turner (1985; see also Ulich 1978) as a result of different spatial distributions of atomic and molecular gas. The inner two or three pixels of our maps (one beam area) is the region of intense star-formation activity, which extends from about 100 to 300 pc in radius, i.e., 7″ to 20″ angular radius, as traced by the infrared (Rieke & Low 1975) and CO (Canzian et al. 1988). The continuum is most intense in this region, but at larger scales it merges smoothly into the extended disk emission (major axis about 10′). A higher resolution study could trace the detailed correspondence of the H I and the structures seen in molecular lines, some of these show distinct noncircular motions which must be associated with the starburst phenomenon.

Using the A array, perhaps in conjunction with VLBI spectroscopy, might reveal the detailed structure of the absorption of the λ21 cm line in front of the continuum. With the resolution of the data presented here it would be premature to analyze the velocity field of the H I in the inner 300 pc. It will clearly be necessary to make a detailed kinematical model of the two or more components of the H I absorption line in order to be confident about the spin temperature and its variation in the nucleus of NGC 253.

5. CONCLUSIONS

The main result from this study is that small scale fluctuations in the emission prevent measuring H I absorption even in nearby galaxies with a beam of 30″, corresponding to 350 pc at an assumed distance of 2.4 Mpc for the Sculptor group. In order to obtain sufficient accuracy in absorption to detect any but the deepest lines will require observations with the A- and/or B-arrays of the VLA (beam sizes 1.″5 and 5″ at λ21 cm). However, the absorption in NGC 247 shown in Figure 6 does appear to be real, and suggests that the gas temperature is below 50 K. This is surprisingly cold by Milky Way standards; very few lines of sight in the solar neighborhood show such cold temperatures.

The nucleus of NGC 253 is so strong in the continuum that the optical depth error due to emission variations is very small. The gas temperature derived from our data is again extremely cold by Milky Way standards. The spin temperature of the lower velocity gas (100 to 220 km s^{-1}) is below 25 K, perhaps as low as 12 K. The higher velocity gas (220 to 320 km s^{-1}) is warmer, about 45 K. This is still cooler than typical atomic clouds in the Milky Way; probably all the H I seen in absorption is associated with the molecular cloud in which the active star formation is taking place.

We are grateful to the NRAO staff for assistance with the observations and reduction of this data, and to Larry Rudnick and Evan Skillman for useful conversations. We are especially grateful to the referee for useful suggestions. This research was supported in part by NSF grant Ast 87-22990 to the University of Minnesota.

REFERENCES

Baan, W. A., Henkel, C., Schilke, P., Mauersberger, R., & Gusten, R. 1990, ApJ, 353, 132
Braun, R. 1990, ApJS, 72, 755
Braun, R., & Walterbos, R. A. M. 1991, ApJ, in press
Canzian, B., Mundy, L. G., & Scoville, N. Z. 1988, ApJ, 333, 157
Carignan, C., & Puche, D. 1990a, AJ, 100, 394
———. 1990b, AJ, 100, 641
Colgan, S., Salpeter, E. E., & Terzian, Y. 1988, ApJ, 328, 275
Combes, F., Gottesman, S. T., & Weliachew, L. 1977, A&A, 59, 181
Corbelli, E., & Schneider, S. E. 1990, ApJ, 356, 14
Dickey, J. M. 1986, ApJ, 300, 190
Dickey, J. M., & Brinks, E. 1988, MNRAS, 233, 781
Dickey, J. M., & Lockman, F. J. 1990, ARA&A, 28, 215
Gardner, F. F., & Whiteoak, J. B. 1974, Nature, 247, 526
Gottesman, S. T., Lucas, R., Weliachew, L., & Wright, M. C. H. 1976, ApJ, 204, 699
Knapp, G. R., & Verschuur, G. L. 1972, AJ, 77, 717
Kuchar, T. A., & Bania, T. 1990, ApJ, 352, 192
Puche, D. 1990, Ph.D. thesis, Univ. Montreal
Puche, D., Carignan, C., & Bosma, A. 1990, AJ, 100, 1468
Puche, D., Carignan, C., & van Gorkom, J. H. 1991, AJ, 101, 456
Puche, D., Carignan, C., & Wainscoat, R. J. 1991, AJ, 101, 447
Puxley, P. J., Hawarden, T. G., & Mountain, C. M. 1990, ApJ, 364, 77
Radhakrishnan, V., Goss, W. M., Murray, J. D., & Brooks, J. W. 1972, ApJS, 24, 49
Rieke, G. H., & Low, F. J. 1975, ApJ, 197, 17
Sage, L. J., Shore, S. N., & Solomon, P. M. 1990, ApJ, 351, 422
Shaya, E. J., & Federman, S. R. 1987, ApJ, 319, 76
Turner, B. E. 1985, ApJ, 299, 312
Turner, J. L., & Ho, P. T. P. 1983, ApJ, 268, L79
Ulich, M.-H. 1978, ApJ, 219, 424
van Gorkom, J. H., Knapp, G. R., Ekers, R. D., Ekers, D. D., Laing, R. A., & Polk, K. S. 1989, AJ, 97, 708